ACS OMEGA

http://pubs.acs.org/journal/acsodf

Article

Conductive Geopolymers as Low-Cost Electrode Materials for Microbial Fuel Cells

Shifan Zhang, Jürgen Schuster, Hanna Frühauf-Wyllie, Serkan Arat, Sandeep Yadav, Jörg J. Schneider, Markus Stöckl,* Neven Ukrainczyk,* and Eddie Koenders

Cite This: *ACS Omega* 2021, 6, 28859−28870

Read Online

ACCESS | Metrics & More | Article Recommendations | Supporting Information

ABSTRACT: Geopolymer (GP) inorganic binders have a superior acid resistance compared to conventional cement (*e.g.*, Portland cement, PC) binders, have better microbial compatibility, and are suitable for introducing electrically conductive additives to improve electron and ion transfer properties. In this study, GP−graphite (GPG) composites and PC−graphite (PCG) composites with a graphite content of 1−10 vol % were prepared and characterized. The electrical conductivity percolation threshold of the GPG and PCG composites was around 7 and 8 vol %, respectively. GPG and PCG composites with a graphite content of 8 to 10 vol % were selected as anode electrodes for the electrochemical analysis in two-chamber polarized microbial fuel cells (MFCs). Graphite electrodes were used as the positive control reference material. *Geobacter sulfurreducens* was used as a biofilm-forming and electroactive model organism for MFC experiments. Compared to the conventional graphite anodes, the anode-respiring biofilms resulted in equal current production on GPG composite anodes, whereas the PCG composites showed a very poor performance. The largest mean value of the measured current densities of a GPG composite used as anodes in MFCs was 380.4 μA cm^{-2} with a standard deviation of 129.5 μA cm^{-2}. Overall, the best results were obtained with electrodes having a relatively low Ohmic resistance, that is, GPG composites and graphite. The very first approach employing sustainable GPs as a low-cost electrode binder material in an MFC showed promising results with the potential to greatly reduce the production costs of MFCs, which would also increase the feasibility of MFC large-scale applications.

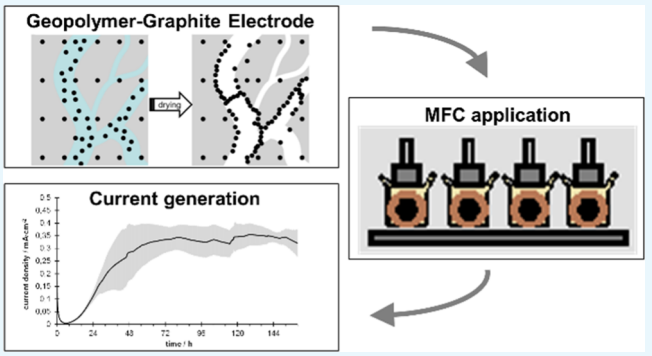

1. INTRODUCTION

Microbial fuel cells (MFCs) represent a very promising technology for sustainable electricity generation from different waste water streams. So far, the power density of MFCs is at least 2 orders of magnitude lower than that of other fuel cells,[1] which represents one of the main drawbacks limiting their commercialization. An effective means of circumventing this disadvantage is large-scale stacking of low-cost MFCs. However, the capital expenditure (CAPEX) has been one of the main issues that have plagued the large-scale application of MFCs. Even with the emergence of membrane-free single-chamber MFCs,[2,3] the cost of the electrodes still accounts for a significant portion of the total cost.[4] Consequently, the development of low-cost electrodes with equivalent power generation efficiency will present new opportunities and directions for the development and commercialization of MFCs.

The anode is key to MFC performance since microbial biofilm formation, substrate oxidation, and the extracellular charge transfer take place here.[5] According to Guo *et al.*, a suitable anode material for MFCs shall provide the following conditions: high electrical conductivity, noncorrosiveness, high surface area, excellent biocompatibility, low costs, ease of fabrication, and scalability.[6] The different types of electrode materials have been reviewed by Kalathil and colleagues in a comprehensive overview.[7] At present, the mainstream anode materials are mainly metal-based[8,9] and carbon-based materials.[10−13] Metal-based materials are comparatively better electrical conductors than carbon-based materials, but their corrosion resistance is less favorable. Carbon-based materials are investigated extensively for their excellent biocompatibility and diversified processing forms.[5] Conventional choices are carbon paper or cloth and graphite plates or rods, while modern types of composite carbon-based anodes have mostly focused to increase the accessible surface area.[14] On the other

Received: July 17, 2021
Accepted: September 27, 2021
Published: October 19, 2021

https://doi.org/10.1021/acsomega.1c03805
ACS Omega 2021, 6, 28859−28870

side, there is a great opportunity to integrate anodes for MFCs into structural materials such as concrete, even at a large structural scale. With regard to the huge volume of a structural element such as wastewater pipes, tanks, and so forth, this integration concept would enable a cost-effective solution for high capacity of power generation, even if the specific energy (per unit mass or volume) is not high.

Geopolymer (GP) is an inorganic amorphous aluminosilicate polymer. The name was coined in 1978 by Professor Joseph Davidovits[15] in France to also indicate that the required raw materials are of widespread geological origin. Nowadays, GPs are considered as upcoming inorganic binders, not only as a sustainable alternative to conventional cements in reducing their CO_2 footprint[15] but also having a great potential for special applications in concrete structures.[16,17] A low calcium content in GPs not only exhibits a vital feature for the acid resistance but also separates them from a broader class of alkali-activated binders.[18,19] Especially in applications where biogenic acid aggressive exposure conditions occur, the use of well-designed GP binders was demonstrated to outperform conventional cement-based binders,[16] along with other technical properties which qualify them for (cement-free) applications as innovative and sustainable construction materials. To obtain the typical GP structure, powder precursors with relatively low proportions of calcium oxide, such as fly ash (byproduct from the coal/biomass burning industry) or calcined clays, are typically activated with liquid alkali−silicate solutions (also called waterglass). Compared to fly ash, metakaolin is more suitable as it exhibits better and more controlled properties, namely, Si/Al ratio and reactivity in alkaline media.[18] The molecular structure of GPs consists of silicate (SiO_4) and aluminate (AlO_4) tetrahedron building blocks, cross-linked by oxygen bridging bonds. The molecular structure can be viewed as an amorphous analogue of zeolites, where a three-dimensional silico-oxide (−Si−O−Si−) and silico-aluminate (−Si−O−Al−O−) network structure is formed by the polycondensation reaction of aluminosilicate oligomers. The negatively charged aluminate tetrahedrons are charge-balanced by alkali metal cations (Na^+ or K^+). The formed GPs are featured by high pore connectivity due to their typical aluminosilicate network,[20] which provides prerequisites for their utilization as anode materials for MFCs. They also have a porous structure, and the pores can absorb water in their natural state so that these materials have a certain ionic conductivity under humid conditions even without the addition of conductive fillers. However, for the application as electrode (anode) materials, improving the electrical conductivity is essential. By forming an electron-conducting network within the GP structure, its conductivity can be significantly increased, which minimizes the Ohmic losses that occur during the use as electrode materials.[21] As mentioned before, an option to increase the GP's conductivity is the application of carbon-based conductive fillers. Natural graphite is an ideal conductive filler material for the production of low-cost, GP-based high-quality electrodes. Its special flake structure helps achieve a low permeation threshold and thus better electrical conductivity. Therefore, natural graphite was used in this study as a conductive filler for the GP materials to be investigated.

In order to demonstrate the practical application of modified GPs as anode materials, the widely applied MFC model organism *Geobacter sulfurreducens* was used as the biocatalyst.[22−24]

2. MATERIALS AND METHODS

2.1. Conductive Electrode. Two types of mortar mixtures, ordinary Portland cement (PC) and GPs, were designed and evaluated to investigate the effects of mixing the two binders with conductive filler materials [PC−graphite (PCG) and GP−graphite (GPG)] on the electrical conductivity and mechanical properties. Described experiments and presented results were obtained at the Department of Materials in Civil Engineering at the Technical University of Darmstadt.

Tap water, standard cement CEM I 42.5N (Heidelberg Cement AG, Germany), and fly ash (class F) were used to prepare PC mortar. Metakaolin and an industrial potassium silicate solution (Supporting Information S1) were used to prepare GP mortar.[18,25] High-purity natural graphite [specific surface area: 10 m^2/g (Supporting Information S2)] was used as electrical conductive fillers. In order to distribute graphite evenly in the mortar, a superplasticizer additive based on polycarboxylate ether was selected as the dispersant.

2.2. Manufacture of PCG and GPG. A standard programmable mortar mixer (E092-01N, Mixmatic, Matest, Italy) was used for the preparation of all test specimens. The fabrication of the samples was carried out in a fully climate-controlled mortar laboratory. The ambient conditions were maintained at 20 °C and 50% relative humidity. Curing and storage of the individual samples were generally carried out in sealed formwork under the same climatic conditions.

Within the scope of this study, 11 different PCG and 12 different GPG paste types (Supporting Information S3) were investigated to analyze the effect of different graphite contents on the electrical conductivity of the two composites and porosity effects. The water−cement ratio (w/c) of PC was 0.6. The graphite volume fractions for the study of PCG conductivity were 0, 1, 3, 4, 8, 9, and 10 vol %. At high graphite content (>5 vol %), the pastes could not be well processed anymore. In contrast, processing was improved by increasing the w/c to 0.75 or by adding fly ash with a mass ratio of 0.3 to cement (f/c = 0.3), with graphite volume fractions of 8, 9, and 10 vol %. The waterglass−metakaolin ratio (wg/mtk) of GPs was 0.8. The graphite volume fractions used to investigate the electrical conductivity of GPG were 0, 1, 3, 5, 7, 8, 9, and 10 vol %. To further improve the porosity of GPG for the utilization as an MFC anode, water with a mass of 1, 1.2, 1.7, and 2 times the graphite content (w/graphite = 1, 1.2, 1.7, and 2) was added to GPG with a volume fraction of 10 vol %. The mixture design is shown in Table 1.

Before starting the mixing process, the inner wall of the mixing bowl from the mortar mixer was wiped with a wet towel. After weighing the required quantity of the raw material, first the polycarboxylate ether (PCE) superplasticiser and water were mixed and repeated three times of washing with water was carried out to avoid any residue caused by the PCE hanging on the walls of the container. Then, the mixture of PCE with water (in the case of GPG, a mixture of water, water glass, and PCE) and graphite was poured into the mixing bowl. Stirring began at a mixing speed of 80 rpm. After 90 s, the stirring speed was increased to 285 rpm for 30 s. Then, the stirring was stopped for 30 s. During this time, the cement powder (metakaolin for GPG) was added. Subsequently, mixing was set to 80 rpm for 180 s and again stopped for 30 s. The inside walls and bottom of the mixer bowl were manually scraped to allow all ingredients to mix well. The mixing was

https://doi.org/10.1021/acsomega.1c03805
ACS Omega 2021, 6, 28859−28870

Table 1. Name and Composition of the Electrode Materials Based on PC and GPs (w, Water; c, Cement; f, Fly Ash; PCE, Superplasticizer; wg, Waterglass; and mtk, Metakaolin)

PCG	w/c in wt %	f/c in wt %	graphite (G) in vol %	PCE/graphite in wt %
PC ref.	0.6	0	0	0
PC06 1C	0.6	0	1	0
PC06 3C	0.6	0	3	0
PC06 4C	0.6	0	4	0
PC06 9C	0.6	0	9	0.1
PC06 3F 8C	0.6	0.3	8	0.1
PC06 3F 9C	0.6	0.3	9	0.1
PC06 3F 10C	0.6	0.3	10	0.1
PC75 8C	0.75	0	8	0.1
PC75 9C	0.75	0	9	0.1
OPC75 10C	0.75	0	10	0.1
GP	wg/mtk in wt %	w/graphite in wt %	graphite in vol %	PCE/graphite in wt %
GP ref.	0.8		0	0.1
GP08 1W 1C	0.8	1	1	0.1
GP08 1W 2C	0.8	1	2	0.1
GP08 1W 3C	0.8	1	3	0.1
GP08 1W 5C	0.8	1	5	0.1
GP08 1W 7C	0.8	1	7	0.1
GP08 1W 8C	0.8	1	8	0.1
GP08 1W 9C	0.8	1	9	0.1
GP08 1W 10C	0.8	1	10	0.1
GP08 1.2W 10C	0.8	1.2	10	0.1
GP08 1.7W 10C	0.8	1.7	10	0.1
GP08 2W 10C	0.8	2	10	0.1

then continued at the same mixing speed for 180 s, followed by increasing the mixing speed to 285 rpm for 60 s. At this point, the mixing process was completed. The fresh mortar was introduced into the mold, placed on a shaking table, and vibrated using a frequency of 40 rpm for 40 s to remove air bubbles. The mold was then sealed.

For the PCG and GPG samples, the molds were removed after 28 and 14 days of curing, respectively. Cylindrical specimen blocks with a diameter of 34 mm and a height of 55 mm were obtained. The specimen blocks were cut into discs with a height of 8 mm. Each disc was placed in a 3D printing (Original Prusa i3 MK3S, Prusa3D, Czech Republic) sanding tool and sanded with 80-, 180-, and 280-grit sandpaper to make it flat and smooth. Finally, 500-grit sandpaper was used to rub back and forth five times in the same direction and rotated by 45°. Sanding was carried out for both sides of the specimens. The surface was cleaned with distilled water, dried, and placed in a sealed container for later use.

2.3. Characterization Methods for Hardened PC and GPs. Compressive strength tests were carried out with samples (80 mm × 40 mm × 40 mm) at a loading rate of 2.4 kN/s according to DIN EN 196-1. The four-probe method was chosen to test the DC resistance of all samples.[26] The DC conductivity of PCG and GPG composites was tested in 100% saturated water (samples were placed in deionized water for 1 day until the mass was constant) and under dry conditions (samples were placed in a 105 °C oven for 7 days until the mass was constant), respectively. Laboratory power supplies (Voltcraft HPS-13015, Voltcraft, Germany) were used to provide a 12 V potential difference between the two ends of the samples. A Desktop multimeter (Voltcraft VC650bt, Voltcraft, Germany) and multimeter (Voltcraft vc830, Voltcraft, Germany) were used for current and voltage measurements, respectively. Mercury intrusion pore (MIP) measurements were performed on 28 day cured specimens using a Pascal 140 and 440 mercury intrusion porosimeter (Thermo Fisher, Waltham, MA, USA) as described before.[21] For MIP measurements, samples were dried in an oven at 105 °C until the mass was constant. Graphite particles and the distribution of graphite in GPs were analyzed by scanning electron microscopy (SEM) (Philips XL-30 FEG, Netherlands) using an electron beam at 20 kV as the accelerating voltage. In the case of energy-dispersive spectroscopy (EDS) and the back-scattered electron (bse, 5 segment 16 mm diode) detectors, SEM−bse−EDS (Zeiss EVO LS25, Jena, Germany) was used with the LaB_6 electron source. A polished portion of the graphite GP compound was prepared for collecting EDS images using a silicon drift detector (25 mm^2, 129 eV, silicon nitride window, 1.0 Mcps) (EDAX, AMETEK, Berwyn, USA). The dried cut cross-sections were impregnated with low-viscosity liquid epoxy resin (EPOFIX, Struers, Denmark), nominally 0.6 mPa s, by means of a 20 kPa vacuum impregnation machine (CitoVac from Struers, Ballerup, Denmark). Samples were polished using a semiautomatic polishing machine (LaboSystem, Struers, Denmark), initially using diamond-based discs (hardness range HV 150 to 2000) at 300 rpm rotational speed, followed by a lubricated cloth and polycrystalline diamond spray of, consecutively, 9, 3, and 1 μm sizes using 150 rpm rotation.

2.4. Microbial Fuel Cell. The different electrode materials were applied as the anode in MFCs with *G. sulfurreducens* as the biocatalyst. The described experiments were carried out at the DECHEMA-Research Institute. All used reagents were of analytical grade: NH_4Cl (Merck); Na_2HPO_4, anhydrous (Merck); KCl, ≥99.5% (Carl Roth GmbH & Co. KG); sodium acetate ≥99%, anhydrous (Carl Roth GmbH & Co. KG); $NaHCO_3$ (Merck); disodium fumarate, anhydrous 98% (Sigma-Aldrich Chemie GmbH); gas mixture Aligal 12, 80% N_2 + 20% CO_2 (Air Liquide); and graphite counter electrodes (CEs, PPG86, Eisenhut GmbH & Co. KG).

2.4.1. Cultivation of G. sulfurreducens. Prior to the use as a biocatalyst in MFC experiments, *G. sulfurreducens* was cultivated under heterotrophic and anaerobic conditions employing fumarate respiration. The only electron and carbon source was acetate, with fumarate as an electron acceptor. The cells were cultivated at 30 °C without shaking in 250 mL septum flasks containing 50 mL of growth medium. *G. sulfurreducens* was supplied by the DSMZ (DSM-12127, Leibniz Institute DSMZ—German Collection of Microorganisms and Cell Cultures, Braunschweig, Germany). Growth medium and detailed cultivation conditions have been described by Stöckl *et al.* before.[24]

2.5. Laboratory Electrochemical H-Cell and Experimental Setup. The electrode materials were examined in a modified H-cell setup which can be used in anaerobic applications as described before.[24] The H-cell setup essentially consisted of two modified 100 mL glass bottles, which were connected *via* flanges. In between the glass bottles, a circular proton-exchange membrane (Nafion 117, Sigma-Aldrich, St. Louis, USA) was inserted to separate the working electrode (WE) and CE chambers. The WE was attached *via* a second flange to the WE chamber using a clamp system. The inner diameter of the WE was 2.5 cm (geometrical A_{WE} = 4.9 cm^2). The CE chamber contained a graphite electrode (geometrical

https://doi.org/10.1021/acsomega.1c03805
ACS Omega 2021, 6, 28859−28870

A_{CE} = 20 cm^2). More detailed information and an image of a completely mounted H-cell are provided in Supporting Information S4.

2.6. Precultivation of *G. sulfurreducens* and Electrode Testing. In several measurement series, the electrode materials listed in Table 2 were examined. In addition, graphite (PPG86, Eisenhut GmbH & Co. KG) was investigated as a positive control, as it had already been successfully applied in earlier studies of *G. sulfurreducens* MFCs, providing reproducible results.[24] Since the graphite particles of GP 1W 1C to GP 1W 7C do not form a linked conductive network, their conductivity is relatively low and the resulting Ohmic resistance is too large, making these samples unsuitable for use as anodes. Simultaneously, four MFCs were operated per series with an experiment runtime of 7 days. Of each electrode material, three to five electrodes were tested. In order to minimize preculture effects in the subsequent MFC experiments, *G. sulfurreducens* cultures were grown and employed according to a fixed procedure: a schematic procedure including precultivation and start of the MFC experiments is shown in Figure 1 and a description of the working steps is given in Supporting Information S5.

Table 2. Tested Electrode Materials (the Number of Experiments Carried Out Are Given in Brackets), Mean Values *M* of Ohmic Resistances R_Ω, and Their Standard Deviations SD[a]

electrode material	R_Ω (kΩ), $M \pm SD$	i_{max} (μA cm^{-2}), $M \pm SD$	$\bar{\sigma}_{160}$ (A s cm^{-2}), $M \pm SD$
PC reference (3)	30 ± 17.3		
PC75 0F 8C	2.5 ± 0.5		
PC75 0F 9C	3 ± 1.0		
PC75 0F 10C	3.2 ± 1.6		
PC06 3F 8C (3)	5.1 ± 4.3		
PC06 3F 9C (3)	2 ± 0.01		
PC06 3F 10C (3)	3.9 ± 2.0	2.3 ± 2.3	1.2 ± 1.0
GP reference (3)	2.7 ± 1.2		
GP08 1W 8C (3)	0.8 ± 0.3	148.0 ± 107.1	67.4 ± 49.5
GP08 1W 10C (3)	1 ± 0.01	157.0 ± 42.3	72.0 ± 11.6
GP08 1.2W 10C (3)	0.4 ± 0.2	166.3 ± 52.3	78.2 ± 24.3
GP08 1.7W 10C (5)	0.1 ± 0.04	380.4 ± 129.5	155.9 ± 45.2
GP08 2W 10C (5)	0.1 ± 0.05	356.2 ± 178.2	140.7 ± 58.5
graphite (5)	0.1 ± 0.05	401.3 ± 51.3	144.5 ± 19.9

[a]The mean values *M* of maximum increase in recorded current densities i_{max}, as well as their standard deviations SD, and the mean values *M* of the surface charge densities $\bar{\sigma}_{160}$ during 160 h of operation, and the standard deviation SD of the surface charge densities.

The assembled MFCs were placed on a multiposition magnetic stirrer inside an incubator (H 30, Edmund Bühler GmbH, Hechingen, Germany), as shown in Supporting Information, Figure S7, at a temperature of 30 °C and were operated with a multipotentiostat system from IPS Elektronik GmbH & Co. KG (PGUMOD, Münster, Germany). The H-cells were placed on magnetic stirring plates inside the incubator. The gas supply tubes were connected to cannulas equipped with sterile filters.

Before inoculating the MFCs, the WE chambers were flushed for 90 min with approx. 40−60 mL min^{-1} 80% N_2 + 20% CO_2 to create anoxic conditions. 30 min before the addition of *G. sulfurreducens*, the WE was polarized to a potential of +400 mV *versus* Ag/AgCl/KCl_{sat}. Subsequently, *G. sulfurreducens* was added to reach a final OD_{600} of 0.1 in the anode compartment of the MFC. Experiments were carried out for 160 h. In order to evaluate the current production, the surface charge density σ_{160} was determined from the recorded current density curves referring to the following equation

$$\sigma_{160} = \frac{Q_{160}}{A}$$

with σ_{160} as the measured charge from the beginning of the tests to the point in time of 160 h and *A* as a geometric, electrochemically active electrode area of 4.9 cm^2. Since electrodes were polarized +400 mV *versus* Ag/AgCl to minimize the initial start-up phase, power density values were not derived from the latter experiments.

2.7. Electrochemical Impedance Spectroscopy. Electrochemical impedance spectroscopy (EIS) was used to determine Ohmic resistances (R_Ω) of the examined electrode materials prior to the polarized MFC experiments. The MFCs were connected in the three-electrode mode; thus, the EIS measurements represent R_Ω of the electrode material and the electrolyte solution in between the electrode surface and the tip of the Haber Lugging capillary (15 mm distanced from the anode), which holds the reference electrode.

EIS measurements were carried out at open circuit potential by applying an excitation AC voltage with an amplitude of 10 mV in the frequency range of 100 kHz to 100 mHz. Evaluation of R_Ω was carried out manually in the high frequency range (10−100 kHz) of the measured data. EIS measurements were performed on a Reference 600+ potentiostat (Gamry Instruments, Warminster, USA).

2.8. Electrode and Biofilm Imaging. *2.8.1. Scanning Electron Microscopy.* A FlexSEM 1000 (Hitachi, Japan) variable-pressure SEM instrument fitted with a BSE + SE detector and an EDX Quantax75 (Bruker) was used to image the electrodes after the MFC experiments. The air-dried electrodes were additionally dried in a vacuum chamber at 20 mbar for 20 min and then fixed with graphite tape to a sample stub. The sample stubs were placed directly into the SEM vacuum compartment and examined at an accelerating voltage of 20 kV.

2.8.2. Fluorescence Microscopy. A Leica TCS SP8 confocal laser scanning microscope (Leica Microsystems GmbH, Wetzlar, Germany) equipped with an HC PL Fluotar 5× dry immersion objective (NA 0.15; free-working distance 13.7 mm), an OPSL 488 nm laser (1.5% intensity), with a PMT detector (501−546 nm, gain 781 V, and scanning speed 400 Hz), and a DD 488/552 excitation beam splitter was used for fluorescence imaging of the biofilms formed on the electrodes. Leica software LAS X version 3.5.5 (Leica Microsystems CMS GmbH, Wetzlar, Germany) was used for image evaluation.

At the end of the polarization experiment, the WE was dismounted from the outer H-cell flange and frozen at −20 °C until imaging. Electrodes were thawn and biofilms were stained with 3 μM SYTO 9 green fluorescent nucleic acid stain (Thermo Fisher Scientific Inc., USA) for 15 min in the dark. Stained biofilms were washed once with 0.125 M phosphate buffer (pH = 6.8) to remove the remaining staining solution and imaged as described above.

https://doi.org/10.1021/acsomega.1c03805
ACS Omega 2021, 6, 28859−28870

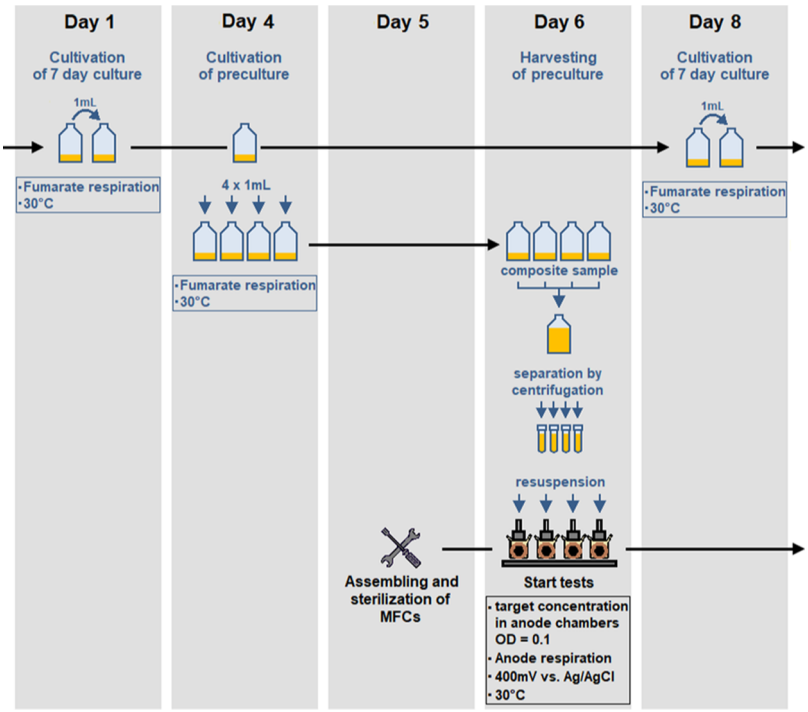

Figure 1. Schematic procedure of *G. sulfurreducens* precultivation and deployment in MFCs. Every 8 days, a fresh 7 day culture was set up. After 3 days of growth to the stationary phase, four fresh cultures were inoculated as precultures for the MFC experiments. In the last step, after another 2 days, the cultivated precultures were combined and cells were harvested by centrifugation and used in the tests with MFCs as the biocatalyst. The cells were cultivated in 250 mL septum flasks containing 50 mL of growth medium. Four MFC experiments were started in parallel. The tests were always started in the same rhythm and ended after max. 7 days.

3. RESULTS AND DISCUSSION

3.1. DC Electrical Conductivity. The electrical conductivity of PCG increases with the addition of graphite content, and the electrical conductivity of PCG (w/c = 0.6) in the saturated state is much higher than that in the dry state. After the graphite content reaches 8 vol %, the water content of graphite does not have a significant effect on the electrical conductivity of PCG, which is stable between 1×10^{-5} and 1×10^{-4} S/m, as shown in Figure 2.

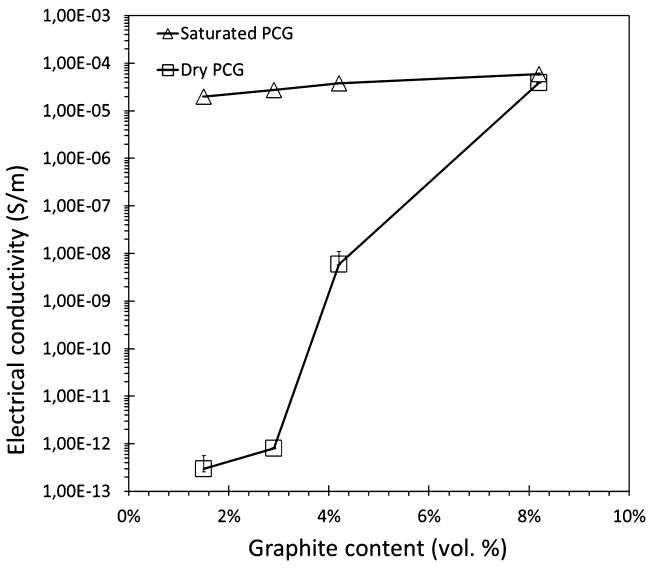

Figure 2. Electric conductivity of PCG (w/c = 0.6) composites with different graphite contents.

The electrical conductivity of GPG (wg/mtk = 0.8 and w/graphite = 1) also increases with the addition of graphite. The conductivity of GPG is spectacularly (several orders of magnitude) higher than that of PCG for the same graphite content. After the graphite content reaches 7 vol %, the electrical conductivity of the dried GPG increases significantly compared to that in the wetted state. At a graphite content of 9 vol %, the conductivity of GPG exceeded 12 S/m. In contrast to the dried specimen, the electrical conductivity of the water-saturated GPG samples under the wet condition varies little with increasing graphite content and only slightly increases in the range of 1−2 S/m. The measured results are shown in Figure 3.

As can be seen, the conductivity of both PCG and GPG increased with the increase in graphite in the mixture. This is mainly attributed to the fact that with increasing graphite content, the contact probability between graphite particles increases. When the percolation (graphite content) threshold is reached, the graphite particles in the mixture form larger clusters, which are interconnected and form a conductive network. The conductive percolation thresholds for dry PCG and GPG are 8 and 7 vol %, respectively. When the graphite content of the mixture exceeds the percolation threshold, the electrical conductivity of the conductive mixture is no longer limited to the ionic conductivity generated by the free ions in the pore solution. The electrical conductivity formed by the interconnected graphite particles in the conductive network likewise contributes to the electrical conductivity of the mixture. Under dry conditions, the samples with graphite content below the percolation threshold clearly lost their electrical conductivity. In contrast, samples with graphite content above the percolation threshold still maintain high

https://doi.org/10.1021/acsomega.1c03805
ACS Omega 2021, 6, 28859−28870

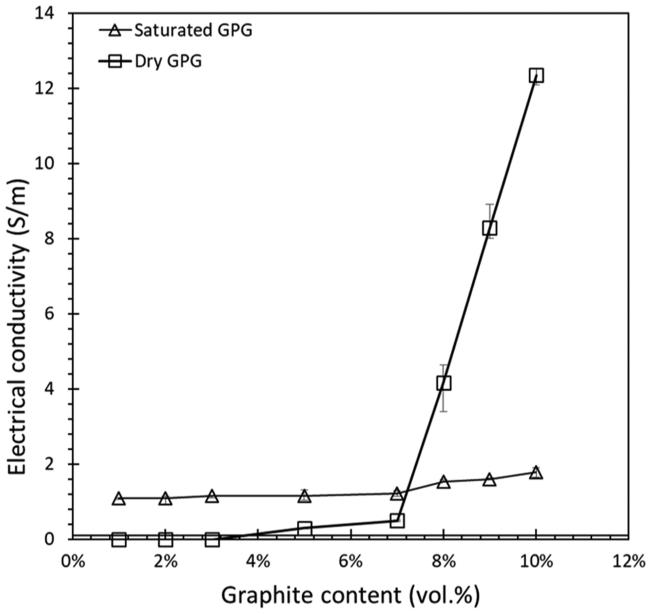

Figure 3. Electric conductivity of GPG (wg/mtk = 0.8 and w/graphite = 1) composites with different graphite contents.

electrical conductivity. For the dried GPG, the electrical conductivity increased significantly after drying (contrary to PCG). A possible explanation for this increase in conductivity is the evaporation of the pore solution during the drying process. The evaporation of the capillary pore solution increases the graphite volume fraction in the solid, which consequently leads to a densification of the particle distribution and eventually to closer spacing between the graphite particles. Figure 4 sketches the assumed aggregation of graphite particles inside the pore structure of the GPG composite, which leads to the formation of conductive bridges. The formation of graphite chains in the dried pore systems is dominated by the smallest particles, being the highest in number distribution. It is also supported by consideration of the different magnitudes of size ratios of the (realistic) pores in the GP (significantly underestimated by MIPs, shown later in Figure 6) and the graphite particles (Figures S1 and S2). Because of the well-known ink-bottle effect, pore sizes detectable by MIP measurements are highly underestimated, due to the filling of the bigger (pore body) pores *via* the smaller pore entry (neck) size, especially in the case of GPs.[28] Alternatively, as graphite particles are also part of the solid matrix, so even if not enough particles could fit into small pores, the drying (shrinkage or heat/chemistry effects) could still promote their aggregation. More research is needed to find the true origin of the observed drying/heating effects.

3.2. Mechanical Properties. In order to be able to assess the practical suitability of the anode material, the compressive strength of the hardened GPG samples was determined by means of a compression test according to DIN EN 196-1.

Figure 5 shows the compressive strength of GPG composites as a function of the volume percentage of graphite. The

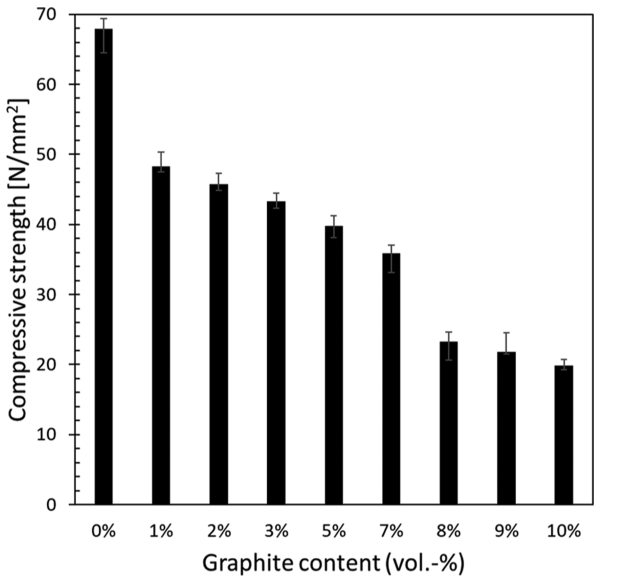

Figure 5. Compressive strengths of hardened GPG samples.

compressive strength is reported as the average value with standard deviation on three different specimens. The compressive strength of the reference samples is 68 N/mm^2. As graphite content increases, the resistance decreases to 20 N/mm^2.

3.3. Morphology and Microstructure Analysis. Pore size distributions of GPG and PCG samples obtained with MIP are shown in Figure 6. A significant difference was found between GPG specimens and PCG specimens. The pore system of GPG can be classified into microcapillaries (pore diameter < 50 nm). The microcapillaries are caused by the evaporation of water in the gel pores.[27] The porosity of microcapillaries also displayed an upward trend from 32 to 50% with an addition of water. In contrast, the pore system of PCG belongs to macrocapillaries (50 nm < pore diameter < 50 μm). The addition of fly ash and graphite particles refines the pore size distribution and results in more pore sizes less than 100 nm, although. However, the majority of pore sizes are still above 50 nm.

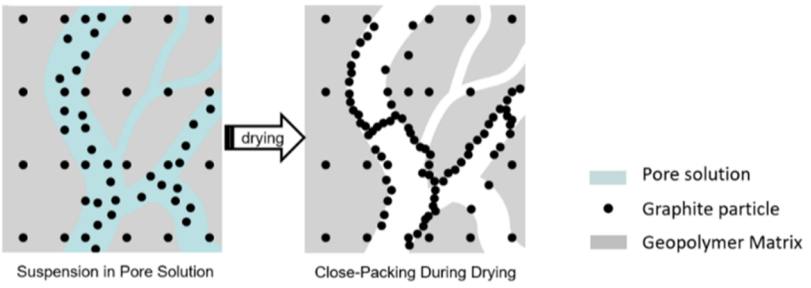

Figure 4. Schematic illustration of the assumed aggregation of graphite particles in GPs during drying.

https://doi.org/10.1021/acsomega.1c03805
ACS Omega 2021, 6, 28859−28870

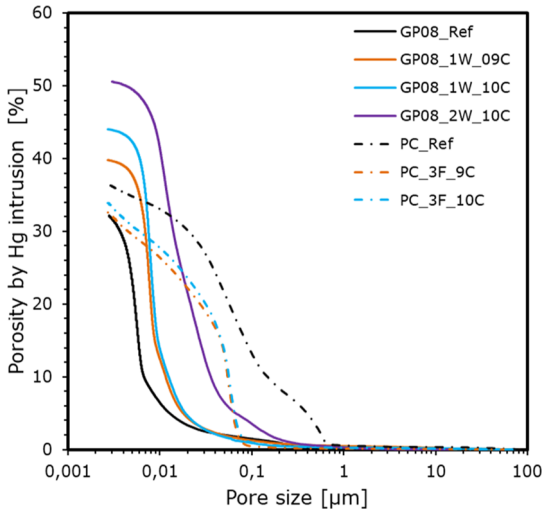

Figure 6. Pore size distribution of the GPG and PCG samples.

The pore size distribution in GPG was mainly concentrated in the range of 3−10 nm. With the increase in water content, the porosity increases, but a majority of the pore sizes are still concentrated in the 10 nm range. As Bhattacharya has mentioned in his book, a distance of 10 nm is still an effective distance for electron tunneling.[28] Therefore, the pores in the GP graphite mixture do not negatively affect the overall conductivity of the mixture. In contrast, the pores therein act as a good separation for the material,[29] enabling the graphite particles in the GPG to be more compactly linked to each other, which further contributes to the electrical conductivity. The pore size distribution in the PCG samples is more extensive compared to the GPG, with most of them being distributed around 50 nm. This prevents electron tunneling from forming in PCG, and the flow of electrons receives a negative effect of the pore structure in PCG. Therefore, the effective electrical conductivity of PCG is much lower than that of GPG.

The SEM micrographs of the GPG samples can be observed in Figure 7, based on graphite sharp edge and platy morphology. As the graphite content increases, the graphite particles in the sample gradually form a continuous conductive network (marked in red shading in Figure 7). It can be assumed from Figure 7d that the GPG composites reach the percolation threshold of 7 vol % of graphite content when the graphite particles constitute a conductive network attached to each other precisely. When the overall graphite content is stabilized at 10 vol % (Figure 7f−h), increasing the porosity of the mixture similarly enables the graphite particles to be more tightly bound to each other, thus enhancing the overall volume fraction of the interconnected portion and improving the electrical conductivity of the GPG composites.

The element distribution of GPG is exemplarily shown for GP08_1W_10C and is illustrated by the EDS elemental mapping in Figure 8, showing the bse gray scaling (inversely proportional to the atomic number, Figure 9a) and individual elements C (carbon), O (oxygen), Al (aluminum), Si (silicon), and K (potassium) separately.

3.4. Electrochemical Cultivation and Electrode Performance. The fabricated PC and GPG electrodes were applied as the anode in a polarized MFC setup with *G. sulfurreducens* as a model organism for 160 h. The results of the MFC experiments are presented below. In Table 2, the results

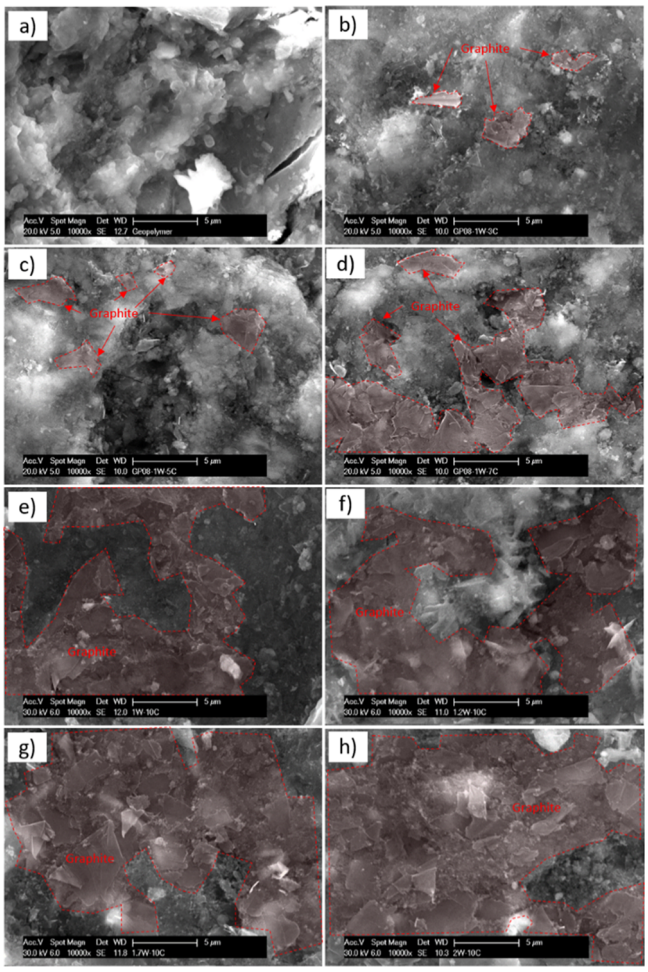

Figure 7. SEM micrographs of samples: (a) GP08_Ref; (b) GP08_1W_3C; (c) GP08_1W_5C; (d) GP08_1W_7C; (e) GP08_1W_10C; (f) GP08_1.2W_10C; (g) GP08_1.7W_10C; and (h) GP08_2W_10C.

of the abiotically resistant measurements with EIS are presented, as well as the maximum currents and the average charge densities of the polarized MFC experiments. In Figure 10, exemplary patterns of the MFC polarization experiments with *G. sulfurreducens* are presented.

Employing the PC electrode materials, it turned out that *G. sulfurreducens* did not produce any current except for the PC063F10C on which a comparatively low maximum current of 2.3 μA cm^{-2} was observed with an average charge density $\overline{\sigma}_{160}$ of 1.2 A s cm^{-2}. A graph of the current density curves of PC electrode materials is provided in Supporting Information S6. Experiments in which no current flow was observed after 24 h were aborted and are not shown.

In contrast to the PC electrodes, a clear trend in performance of *G. sulfurreducens* on GPG electrode materials could be observed depending on the electrode composition. While no anodic current was detected with GPG electrodes with no addition of graphite and no further water content (GP reference), all other GPG electrode materials generated significant currents. The mean current density curves (black) including standard deviations (gray) of *G. sulfurreducens* on the different GPG electrodes with varying graphite and water contents and results of the graphite electrodes (positive control) are presented in Table 2 and Figure 9.

https://doi.org/10.1021/acsomega.1c03805
ACS Omega 2021, 6, 28859−28870

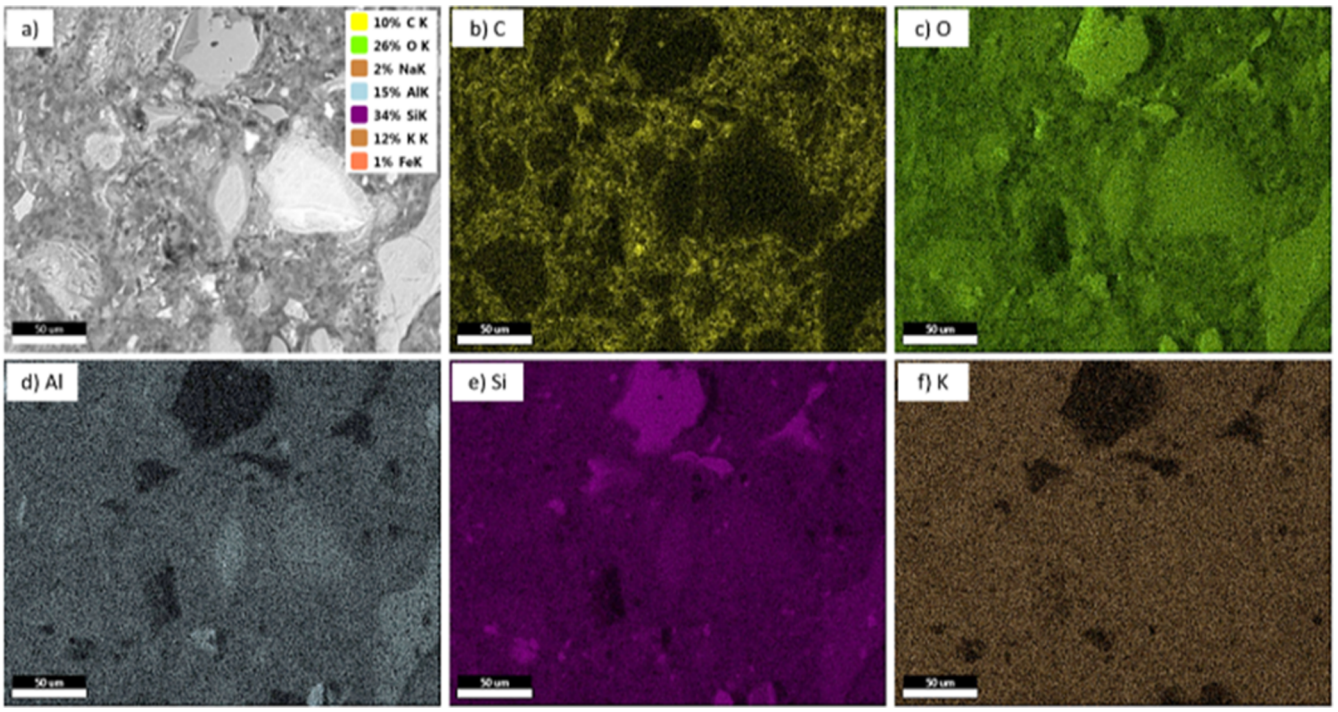

Figure 8. Elemental distribution (color) of GP08_1W_10C. (a) bse detector. EDS detector: (b) elements C: carbon; (c) elements O: oxygen; (d) elements Al: aluminum; (e) elements Si: silicon; and (f) elements K: potassium.

In general, the performance outline of *G. sulfurreducens* on different electrode materials can be given with the Ohmic resistances of the electrodes (which were measured before inoculation of the bacteria), together with the charge density σ_{160}, the total amount of charge that they produced during the tests within 160 h.

The best performance of the anode-respiring biofilms was shown on the reference graphite electrodes and GPG electrodes with a graphite content of 10 vol % and a water/graphite ratio of 1.7 and 2. Similar behavior was observed with these three types of electrodes, whose highest current densities (449−571 μA cm^{-2}) were reached after about 72 h with the highest surface charge densities σ_{160}, in a range of approx. 140−156 A s cm^{-2}.

With regard to the GPG electrode material, the graphite content of 10 vol % is not the decisive factor for MFC performance but the water/graphite ratio. Increasing water/graphite ratios with a constant graphite content of 10 vol % led to a drop in R_Ω. GPG electrode materials with a ratio of 1.7 and 2 showed the same R_Ω of around 0.1 kΩ, comparable to graphite electrodes, which is most probably attributed to the electrolyte resistance. However, as the water/graphite ratio increases, the electrodes become more porous and fragile, indicating stability limitations for further material improvement. These properties are the main difference to the positive control material graphite, with its nonporous structure and high stability.

MFCs employing GPG electrodes with a water/graphite ratio lower than 1.7 and consequently higher Ohmic resistances showed significantly lower current densities. Therefore, we conclude that the performance of the electrode material in MFCs mainly depends on the resistances of the electrode material.

Due to the different porosities of the GPG electrode materials, the medium in the anode chamber partly leaked through the electrodes during the tests, which led to a decrease in the fill levels of the medium, which were different for all electrodes. The fill levels were checked regularly and equalized by the addition of fresh and anoxic *Geobacter* medium without fumarate. By equalizing the fill levels in the MFCs, new substrate was added to the cultures which probably caused the observed current density plateaus, as can be seen in Figure 9 (curves A to E). In contrast, no medium was added to anode chambers containing the nonporous graphite electrodes. Hence, in these experiments, substrate concentration decreased over time, which most probably caused the decrease in current density after 72 h (Figure 9F).

Besides the decreasing substrate concentration, a decrease in pH within the biofilm due to proton accumulation over time is also thought to reduce biological activity,[30] which however would be true for the GP electrodes as well.

In summary, GPG electrodes were successfully applied as the anode material in polarized MFC experiments, whereas PC electrodes showed no or an inferior performance compared to GPG. With increasing water content (1.7W and 2W), the performance of GPG electrodes improves and current densities and surface charge densities, which are comparable to graphite electrodes, can be achieved. Due to continuous supply of fresh medium (and thereby the substrate) for GPG electrodes, the current density during 160 h of operation remains stable for electrodes GP08 2W 10C and GP08 1.7W 10C compared to graphite electrodes. When comparing electrode performances, the distinct available electrode surface caused by different porosities of the materials is not taken into account. Insights into the electrode surface structure are given in the following section.

3.5. CLSM and SEM Imaging. In order to illustrate both surface morphology and biofilm formation by *G. sulfurreducens* during MFC experiments on the electrode materials, four exemplary electrodes were imaged, and the respective images

https://doi.org/10.1021/acsomega.1c03805
ACS Omega 2021, 6, 28859−28870

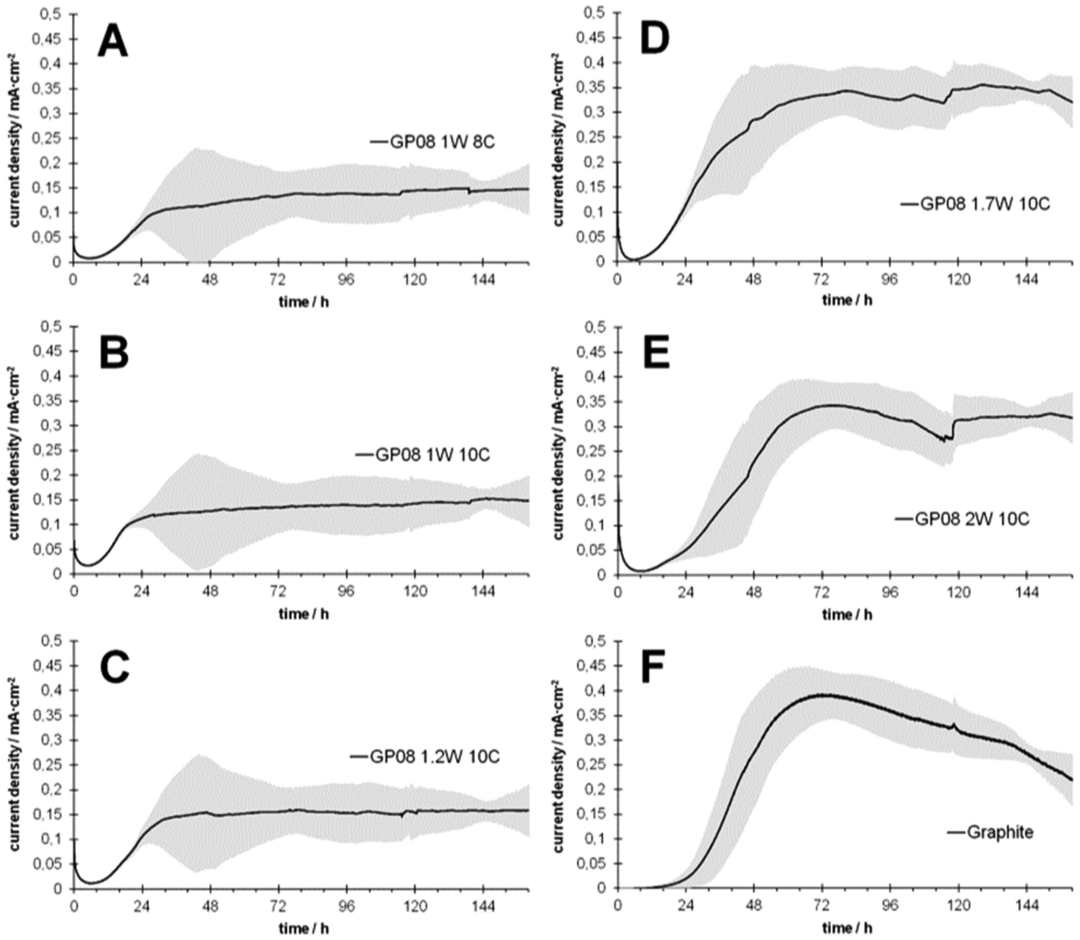

Figure 9. Mean current density curves for cultivations of *G. sulfurreducens* in H-cell MFCs on different GP electrodes with variable graphite and water content, as well as MFCs on graphite electrodes (anoxic *Geobacter* medium with acetate and without fumarate; electron acceptor: anode; 30 °C; anaerobic). Current density is referred to the geometrical WE surface (4.9 cm^2). Standard deviations (of 3 to 5 individual runs) are shown in gray. Electrode types: (A) GP08 1W 8C, (B) GP08 1W 10C, (C) GP08 1.2W 10C, (D) GP08 1.7W 10C, (E) GP08 2W 10C, and (F) reference graphite electrode.

are presented in Figure 10. SEM images were taken prior to MFC experiments of fresh electrodes in order to visualize surface morphology on the μm-scale. Photographs of the electrodes and images with a fluorescence microscope were taken after MFC experiments in order to illustrate bacterial biofilm formation. Biofilms were stained with the fluorescent DNA staining dye SYTO 9. In the SEM images, GP08 2W 10C and graphite show similar surface roughness which is mainly due to the structure of the graphite contained. However, the morphology of the deposited biofilm is rather different: smooth for the graphite grown biofilm and nonuniform on the GP08 2W 10C electrode. Nevertheless, both biofilms performed similarly in the MFC, which means one cannot conclude the MFC performance of an electrode material from biofilm morphology. PC06 3F 8C and GP reference both appear less granulated in the SEM images and show biomass deposition as well, even though no current was produced. Biomass deposition without current generation on the anode can indicate that another electron acceptor than the electrode was present. Since fumarate was omitted, residual oxygen present in the medium or diffusing through the porous anodes might have served as an electron acceptor for *G. sulfurreducens*. Formerly classified as an obligate anaerobic bacterium, studies now showed that it can tolerate little amount of oxygen and even use it as an electron acceptor.[31] If oxygen diffuses through the electrode and accumulates on the electrode surface, biofilm formation might be possible even if the electrode is not used as an electron sink. In general, one might have seen a difference in the quantity of the biofilm formed on the electrode between current-producing and nonproducing materials, but since the electrodes were frozen before imaging, no biofilm quantification was possible. Nevertheless, the tested materials all seem to be biocompatible.

4. CONCLUSIONS

GPG composites with different graphite contents were investigated focusing on the effect of microstructural changes on the electrical conductivity. The critical factor for the GPG blends to reach a high electrical conductivity is the formation of interconnected conductive networks of graphite particles in the GP matrix. At this point, the conductive mechanism of the mixture no longer relies on ionic conductivity but rather on electronic conductivity between the graphite particles. The large number of small graphite particles located in pore spaces allows the GPG mixtures above the percolation threshold to possess a stable conductivity in the dry case, even exceeding the conductivity of the mixture in the wet state. The conductivity of the mixture continues to increase by increasing the porosity of the system, while the graphite volume fraction remains constant at 10 vol %. This is mainly due to the fact

https://doi.org/10.1021/acsomega.1c03805
ACS Omega 2021, 6, 28859−28870

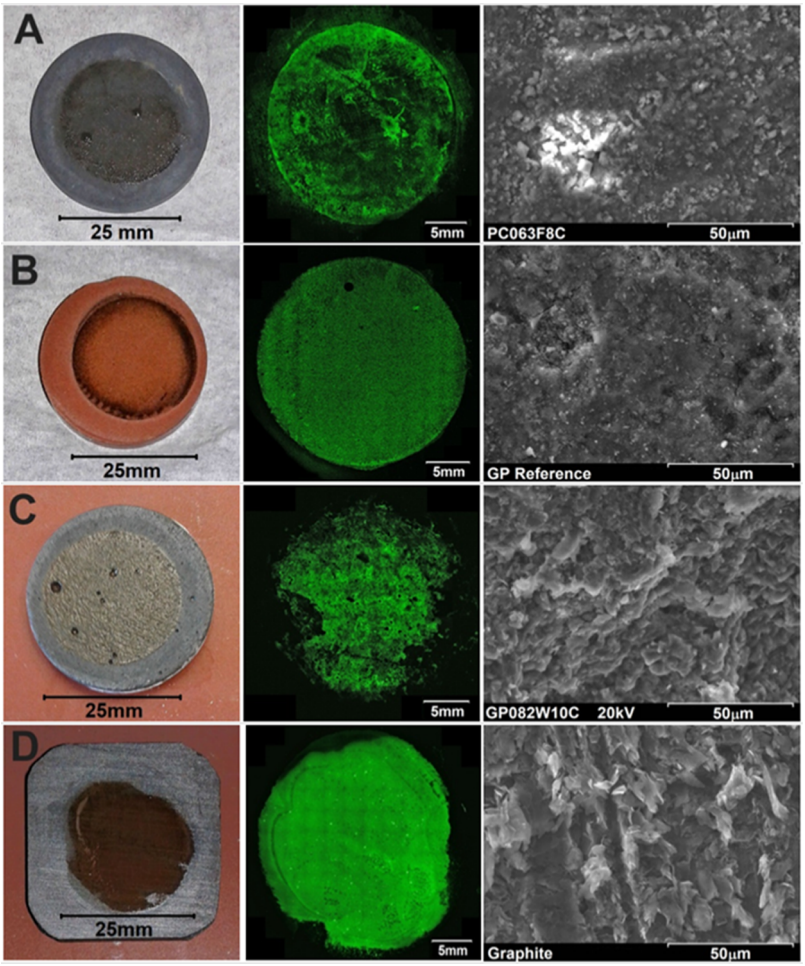

Figure 10. Four different electrode materials after application as anodes in polarized MFC experiments are shown. From left to right depicted: photograph of the electrode, CLSM image of the SYTO 9-stained biofilm, and SEM image of the fresh electrode surface without the biofilm. (A) PC06 3F 8C which produced no current. (B) GP reference which as well produced no current. (C) GP08 2W 10C electrode. (D) Reference graphite electrode.

that the pores act as separators in the system, thus allowing the graphite particles to be more tightly interconnected.

Any GPG anode with graphite content above the percolation threshold can be used as an MFC anode, and as the graphite content increases, the conductivity increases and so does the current density of the MFC. Since the biocompatibility of GPC electrodes has been shown with the presented experiments but still no current was produced in the respective MFCs, further electrode optimization based on the determination of the Ohmic resistance is suggested. Increasing the porosity of the GPG compound provides more sample space for microorganisms to attach to and increases the electrochemically active surface, in addition to improved electrical conductivity of the mixture. Thereby, GPG anodes with high water content remarkably result in a similar current output compared to the graphite electrodes used as the positive control. Biofilm imaging immediately after the end of the experiment and applying Live/Dead staining could give additional insights into biomass−anode interaction in future experiments.

With this publication, the authors present the very first approach employing sustainable GPs as low-cost electrode binder materials in a polarized MFC. The results demonstrate the great potential to reduce the production costs of electrode materials for MFCs, which would also increase the feasibility of MFC large-scale applications.

■ ASSOCIATED CONTENT

Supporting Information

The Supporting Information is available free of charge at https://pubs.acs.org/doi/10.1021/acsomega.1c03805.

Metakaolin and waterglass raw materials; graphite powder raw material; mixture design of PCG and GPG; laboratory electrochemical H-cell; description of the working steps of the MFC experiments; current density curves of tests; and photograph of the multi-MFC setup (PDF)

■ AUTHOR INFORMATION

Corresponding Authors

Markus Stöckl − *Department of Electrochemistry, DECHEMA-Research Institute, 60486 Frankfurt a. M., Germany*; Email: markus.stoeckl@dechema.de

Neven Ukrainczyk − *Department of Materials in Civil Engineering at the Technical University of Darmstadt, 64287 Darmstadt, Germany*; orcid.org/0000-0003-4122-0547; Email: ukrainczyk@wib.tu-darmstadt.de

https://doi.org/10.1021/acsomega.1c03805
ACS Omega 2021, 6, 28859−28870

Authors

Shifan Zhang − *Department of Materials in Civil Engineering at the Technical University of Darmstadt, 64287 Darmstadt, Germany*

Jürgen Schuster − *Department of Electrochemistry, DECHEMA-Research Institute, 60486 Frankfurt a. M., Germany*

Hanna Frühauf-Wyllie − *Department of Industrial Biotechnology, DECHEMA-Research Institute, 60486 Frankfurt a. M., Germany*

Serkan Arat − *Department of Corrosion, DECHEMA-Research Institute, 60486 Frankfurt a. M., Germany*

Sandeep Yadav − *Department of Chemistry at the Technical University of Darmstadt, 64287 Darmstadt, Germany*

Jörg J. Schneider − *Department of Chemistry at the Technical University of Darmstadt, 64287 Darmstadt, Germany*

Eddie Koenders − *Department of Materials in Civil Engineering at the Technical University of Darmstadt, 64287 Darmstadt, Germany*

Complete contact information is available at: https://pubs.acs.org/10.1021/acsomega.1c03805

Notes

The authors declare no competing financial interest.

■ ACKNOWLEDGMENTS

The authors gratefully acknowledge the financial support of the Research Initiative "Zukunft Bau" of the Federal Institute for Building, Urban and Regional Research (project: SWD-10.08.18.7-18.25) and the project "PV-WALL" PZS-2019-02-1555 in Research Cooperability Program of the Croatian Science Foundation funded by the European Union. The authors also acknowledge support by the Deutsche Forschungsgemeinschaft (DFG − German Research Foundation) and the Open Access Publishing Fund of Technische Universität Darmstadt.

■ REFERENCES

(1) Ren, H.; Tian, H.; Gardner, C. L.; Ren, T.-L.; Chae, J. A Miniaturized Microbial Fuel Cell with Three-Dimensional Graphene Macroporous Scaffold Anode Demonstrating a Record Power Density of over 10 000 W m $^{-3}$. *Nanoscale* **2016**, *8*, 3539−3547.

(2) Liu, H.; Logan, B. E. Electricity Generation Using an Air-Cathode Single Chamber Microbial Fuel Cell in the Presence and Absence of a Proton Exchange Membrane. *Environ. Sci. Technol.* **2004**, *38*, 4040−4046.

(3) Liu, H.; Cheng, S.; Huang, L.; Logan, B. E. Scale-up of Membrane-Free Single-Chamber Microbial Fuel Cells. *J. Power Sources* **2008**, *179*, 274−279.

(4) Yaqoob, A. A.; Ibrahim, M. N. M.; Rodríguez-Couto, S. Development and Modification of Materials to Build Cost-Effective Anodes for Microbial Fuel Cells (MFCs): An Overview. *Biochem. Eng. J.* **2020**, *164*, 107779.

(5) Kerzenmacher, S. Engineering of Microbial Electrodes. In *Bioelectrosynthesis*; Harnisch, F., Holtmann, D., Eds.; Advances in Biochemical Engineering/Biotechnology; Springer International Publishing: Cham, 2017; Vol. *167*, pp 135−180.

(6) Guo, K.; Prévoteau, A.; Patil, S. A.; Rabaey, K. Engineering Electrodes for Microbial Electrocatalysis. *Curr. Opin. Biotechnol.* **2015**, *33*, 149−156.

(7) Kalathil, S.; Patil, S. A.; Pant, D. Microbial Fuel Cells: Electrode Materials. In *Encyclopedia of Interfacial Chemistry*; Elsevier, 2018; pp 309−318.

(8) Guo, K.; Donose, B. C.; Soeriyadi, A. H.; Prévoteau, A.; Patil, S. A.; Freguia, S.; Gooding, J. J.; Rabaey, K. Flame Oxidation of Stainless Steel Felt Enhances Anodic Biofilm Formation and Current Output in Bioelectrochemical Systems. *Environ. Sci. Technol.* **2014**, *48*, 7151−7156.

(9) Baudler, A.; Schmidt, I.; Langner, M.; Greiner, A.; Schröder, U. Does It Have to Be Carbon? Metal Anodes in Microbial Fuel Cells and Related Bioelectrochemical Systems. *Energy Environ. Sci.* **2015**, *8*, 2048−2055.

(10) Bueche, F. Electrical Properties of Carbon Black in an SBR−Wax Matrix. *J. Polym. Sci., Part A-2* **1973**, *11*, 1319−1330.

(11) Chen, S.; Hou, H.; Harnisch, F.; Patil, S. A.; Carmona-Martinez, A. A.; Agarwal, S.; Zhang, Y.; Sinha-Ray, S.; Yarin, A. L.; Greiner, A.; Schröder, U. Electrospun and Solution Blown Three-Dimensional Carbon Fiber Nonwovens for Application as Electrodes in Microbial Fuel Cells. *Energy Environ. Sci.* **2011**, *4*, 1417.

(12) Lu, Z.-K.; Fu, Y.-B.; Xu, Q.; Liu, Y.-Y.; Zhang, Y.-L. Application of Modified Foam Graphite Anode with Low Potential in Marine Benthic Microbial Fuel Cell. *J. Inorg. Mater.* **2013**, *28*, 278−282.

(13) Logan, B.; Cheng, S.; Watson, V.; Estadt, G. Graphite Fiber Brush Anodes for Increased Power Production in Air-Cathode Microbial Fuel Cells. *Environ. Sci. Technol.* **2007**, *41*, 3341−3346.

(14) Sonawane, J. M.; Yadav, A.; Ghosh, P. C.; Adeloju, S. B. Recent Advances in the Development and Utilization of Modern Anode Materials for High Performance Microbial Fuel Cells. *Biosens. Bioelectron.* **2017**, *90*, 558−576.

(15) Davidovits, J. Environmental Implications of Geopolymers. *Mater. Today* **2015**, https://www.materialstoday.com/polymers-soft-materials/features/environmental-implications-of-geopolymers (accessed Oct 4, 2021).

(16) Grengg, C.; Ukrainczyk, N.; Koraimann, G.; Mueller, B.; Dietzel, M.; Mittermayr, F. Long-Term in Situ Performance of Geopolymer, Calcium Aluminate and Portland Cement-Based Materials Exposed to Microbially Induced Acid Corrosion. *Cem. Concr. Res.* **2020**, *131*, 106034.

(17) Grengg, C.; Mittermayr, F.; Ukrainczyk, N.; Koraimann, G.; Kienesberger, S.; Dietzel, M. Advances in Concrete Materials for Sewer Systems Affected by Microbial Induced Concrete Corrosion: A Review. *Water Res.* **2018**, *134*, 341−352.

(18) Vogt, O.; Ukrainczyk, N.; Ballschmiede, C.; Koenders, E. A. B. Reactivity and Microstructure of Metakaolin Based Geopolymers: Effect of Fly Ash and Liquid/Solid Contents. *Materials* **2019**, *12*, 3485.

(19) Ukrainczyk, N. Simple Model for Alkali Leaching from Geopolymers: Effects of Raw Materials and Acetic Acid Concentration on Apparent Diffusion Coefficient. *Materials* **2021**, *14*, 1425.

(20) Ukrainczyk, N.; Muthu, M.; Vogt, O.; Koenders, E. Geopolymer, Calcium Aluminate, and Portland Cement-Based Mortars: Comparing Degradation Using Acetic Acid. *Materials* **2019**, *12*, 3115.

(21) Logan, B. E.; Hamelers, B.; Rozendal, R.; Schröder, U.; Keller, J.; Freguia, S.; Aelterman, P.; Verstraete, W.; Rabaey, K. Microbial Fuel Cells: Methodology and Technology. *Environ. Sci. Technol.* **2006**, *40*, 5181−5192.

(22) Bond, D. R.; Holmes, D. E.; Tender, L. M.; Lovley, D. R. Electrode-Reducing Microorganisms That Harvest Energy from Marine Sediments. *Science* **2002**, *295*, 483−485.

(23) Bond, D. R.; Lovley, D. R. Electricity Production by Geobacter Sulfurreducens Attached to Electrodes. *Appl. Environ. Microbiol.* **2003**, *69*, 1548−1555.

(24) Stöckl, M.; Teubner, N. C.; Holtmann, D.; Mangold, K.-M.; Sand, W. Extracellular Polymeric Substances from *Geobacter Sulfurreducens* Biofilms in Microbial Fuel Cells. *ACS Appl. Mater. Interfaces* **2019**, *11*, 8961−8968.

(25) Vogt, O.; Ballschmiede, C.; Ukrainczyk, N.; Koenders, E. Evaluation of Sulfuric Acid-Induced Degradation of Potassium Silicate Activated Metakaolin Geopolymers by Semi-Quantitative SEM-EDX Analysis. *Materials* **2020**, *13*, 4522.

(26) Han, B.; Ding, S.; Yu, X. Intrinsic Self-Sensing Concrete and Structures: A Review. *Measurement* **2015**, *59*, 110−128.

(27) Cui, Y.; Wang, D. Effects of Water on Pore Structure and Thermal Conductivity of Fly Ash-Based Foam Geopolymers. *Adv. Mater. Sci. Eng.* **2019**, *2019*, 1−10.
(28) Bhattacharya, S. K. *Metal Filled Polymers*; Plastics Engineering; Taylor & Francis, 1986.
(29) Park, S.-H.; Hwang, J.; Park, G.-S.; Ha, J.-H.; Zhang, M.; Kim, D.; Yun, D.-J.; Lee, S.; Lee, S. H. Modeling the Electrical Resistivity of Polymer Composites with Segregated Structures. *Nat. Commun.* **2019**, *10*, 2537.
(30) Franks, A. E.; Nevin, K. P.; Jia, H.; Izallalen, M.; Woodard, T. L.; Lovley, D. R. Novel Strategy for Three-Dimensional Real-Time Imaging of Microbial Fuel Cell Communities: Monitoring the Inhibitory Effects of Proton Accumulation within the Anode Biofilm. *Energy Environ. Sci.* **2009**, *2*, 113−119.
(31) Engel, C. E. A.; Vorländer, D.; Biedendieck, R.; Krull, R.; Dohnt, K. Quantification of Microaerobic Growth of Geobacter Sulfurreducens. *PLoS One* **2020**, *15*, No. e0215341.

https://doi.org/10.1021/acsomega.1c03805
ACS Omega 2021, 6, 28859−28870